Supersonic External-Compression Inlets for Mach 1.4 to 2.0

John W. Slater[1]
John H. Glenn Research Center, Cleveland, Ohio, 44135, USA

A series of supersonic, external-compression inlets were designed for freestream Mach numbers of Mach 1.4, 1.7, and 2.0. The types of inlets included axisymmetric pitot, axisymmetric spike, two-dimensional, two-dimensional bifurcated, and streamline-traced inlets. The inlets were designed as isolated from the airframe with freestream conditions, engine-face geometry, and flow rates established from a reference NASA commercial aircraft concept. The inlets were designed using the NASA Supersonic Inlet Design and Analysis (SUPIN) Tool and the inlet performance was obtained from computational fluid dynamics (CFD) simulations. The study compares the physical dimensions and aerodynamic performance of the inlets to provide reference information for the selection of inlet types for commercial supersonic aircraft.

Nomenclature

A	=	Cross-sectional area
A_2*	=	Cross-sectional area at the engine face based on D_2 without area accounting for the hub / spinner
C_{Dwave}	=	Cowl exterior wave drag coefficient
D	=	Diameter
D_{hub}	=	Diameter of the hub or spinner at the engine face
D_{noz}	=	Diameter of the throat of the outflow nozzle
Δy_{focal}	=	Vertical offset of the focal point from the cowl lip point
DPC/P	=	Circumferential total pressure distortion intensity
DPR/P	=	Radial total pressure distortion intensity
h	=	Height
h_0	=	Altitude for the freestream
h_{plen}	=	Height of the bleed slot plenum
L	=	Length
L_{cb1sh}	=	Length from the end of the external supersonic diffuser to the start of the shoulder / bleed slot
L_{exd}	=	Length of the external supersonic diffuser
L_{inlet}	=	Length of the inlet
L_{plen}	=	Length of the bleed slot plenum
L_{shSD}	=	Length from the end of the shoulder / bleed slot to the start of the subsonic diffuser
L_{slot}	=	Length of the shoulder / bleed slot
L_{subd}	=	Length of the subsonic diffuser
L_{thrt}	=	Length of the throat section
M	=	Mach number
M_{EX}	=	Supersonic Mach number at the end of the external supersonic diffuser
N_{stgs}	=	Number of stages for the external supersonic diffuser
p	=	Static pressure
p_t	=	Total pressure
θ	=	Slope
θ_{eqSD}	=	Equivalent conical angle for the subsonic diffuser
$\theta_{stg\#}$	=	Slopes for the stages of the external supersonic diffuser with # = (1,2,3)

[1] Research Aerospace Engineer, Propulsion Division / Inlets and Nozzles Branch, AIAA Associate Fellow.

S = Surface area
S_{comp} = Compressive area of an inlet
S_{cwexx} = Surface area of a cowl exterior projected to an axial plane
S_{inlet} = Total surface area of an inlet
w_{cap} = Width of the capture cross-section for the two-dimensional inlets
W = Flow rate
W_{bleed} = Flow rate of bleed
W_{C2} = Altitude-adjusted corrected flow rate at the engine face
$W_{spillage}$ = Flow rate of supersonic and subsonic spillage
x, y, z = Cartesian coordinates
$(x,y,\theta)_{cb1}$ = Planar coordinates and slope on the centerbody at the endpoint of the external supersonic diffuser
$(x,y,\theta)_{cbTS}$ = Planar coordinates and slope on the centerbody at the shoulder point
$(x,y,\theta)_{cbSD}$ = Planar coordinates and slope on the centerbody at the start of the subsonic diffuser
$(x,y,\theta)_{clip}$ = Planar coordinates and slope of the cowl lip point
$(x,y,\theta)_{clin}$ = Planar coordinates and slope at the cowl lip interior point
$(x,y,\theta)_{clex}$ = Planar coordinates and slope at the cowl lip exterior point
$(x,y,\theta)_{cwTS}$ = Planar coordinates and slope on the cowl interior at the shoulder point
$(x,y,\theta)_{cwSD}$ = Planar coordinates and slope on the cowl interior at the start of the subsonic diffuser
$x_{stg\#}$ = x-coordinates for the endpoints for the stages of the external supersonic diffuser with # = (1,2,3)
$(\,)_0$ = Freestream property
$(\,)_1$ = Property at the cowl lip / inlet entrance station
$(\,)_2$ = Property at the engine-face station
$(\,)_{cap}$ = Property associated with the reference capture area
$(\,)_{SD}$ = Property at station SD, start of the subsonic diffuser
$(\,)_{TS}$ = Property at station TS, shoulder of the throat section

I. Introduction

Commercial supersonic aircraft require an efficient propulsion system consisting of an inlet, engine, and nozzle integrated well with the airframe. The primary design point for the propulsion system of a commercial supersonic aircraft is the cruise condition, as this is the condition at which the aircraft spends most of its flight time. The focus of this paper is on the aerodynamic design of the inlets for aircraft envisioned to cruise at Mach numbers from Mach 1.4 to 2.0.

The design of the inlet requires specification of the flow conditions approaching the inlet and the physical dimensions and flow rate at the engine face, which is the interface of the inlet with the engine. For this study, this information was obtained from consideration of the NASA Supersonic Technology Concept Aeroplane (STCA) [1]. The STCA is a 55-ton business-class airplane concept powered by three turbofan engines and designed to perform transatlantic flights with 8 passengers at a cruise of Mach 1.4. The STCA study also included a conceptual design of a low-bypass turbofan engine, which is used for the inlet design studies of this paper.

A primary task of an inlet is the deceleration of the supersonic flow captured by the inlet to the subsonic conditions required by the engine. The deceleration of the inlet flow results in compression of the flow which contributes to the compression leg of the propulsion cycle. The deceleration and compression is performed using a shock system that at its outflow creates subsonic flow which is further decelerated by a subsonic diffuser to achieve the subsonic Mach number desired at the engine face. For cruise Mach numbers at or below Mach 2.0, a shock system external to the inlet interior duct is regarded as the appropriate choice based on the desire for an efficient yet stable shock system. Thus, the inlets studied and discussed within this paper are external-compression inlets.

The design of the inlet includes a selection of the type of inlet with the possible options being a pitot, axisymmetric-spike, two-dimensional, two-dimensional bifurcated-duct, or streamline-traced inlet. The choice of inlet type will affect the physical dimensions (i.e., lengths, diameters, surface areas) of the inlet. A design goal is to minimize the physical dimensions of the inlet to keep the weight and aerodynamic drag at a minimum.

This study explored the variation of the physical dimensions and aerodynamic performance of the five inlet types at freestream Mach numbers of Mach 1.4, 1.7, and 2.0. The aerodynamic performance was characterized by the flow rates about and through the inlets, the total-pressure recovery and distortion at the engine face, and wave drag. It was assumed in this study that the inlets would be integrated with the airframe such that the flow approaching the inlet would be uniform and not adversely affected by the inlet-airframe integration. Thus, the inlets were designed to be

isolated from the airframe with the flow approaching the inlet at the being the same as the freestream conditions approaching the aircraft.

This study built upon previous inlet design studies performed by the author and colleagues. Reference [2] studied two-dimensional inlets for the Mach range of interest. Reference [3] discussed the design of an axisymmetric spike inlet for Mach 1.4. References [4] and [5] discussed the design of a streamline-traced, external-compression inlet for Mach 1.7 and 2.0, respectively. Reference [6] discussed a study of the two-dimensional inlet for the Concorde.

A description of the inlet types and inlets included within the study of this paper is presented in Section II. The geometry models used for the design of the external supersonic diffusers, throat section, and subsonic diffuser are described and the important design factors are identified. The design of the inlets was facilitated using the NASA Supersonic Inlet Design and Analysis (SUPIN) Tool [7], which is also briefly described in Section II. While SUPIN does provide estimates of the inlet aerodynamic performance, computational fluid dynamics (CFD) simulations were used to obtain higher fidelity estimates of the inlet performance. Section III describes the computational grids and methods used for the CFD simulations. Section IV presents a summary of the fifteen inlets designed and simulated as part of this study which include the combinations of the five inlet types and three freestream Mach numbers. The physical dimensions and aerodynamic performance of the inlets are presented and compared. Each inlet was designed for the respective cruise design condition and the aerodynamic performance metrics at this operating point are compared. The characteristic curves for the variations of the total pressure recovery and distortion as the engine flow ratio was varied are also presented.

II. Descriptions of the Inlets

This section describes the physical features, freestream and engine-face conditions, and geometry models for the five inlet types of the study.

A. Inlet Types

This study explored the use of axisymmetric pitot, axisymmetric spike, two-dimensional, two-dimensional bifurcated, and streamline-traced inlets for a commercial supersonic aircraft. Figure 1 shows images of the five inlet types designed for Mach 1.7. All the inlets were external-compression inlets and were designed for the same engine-face diameter.

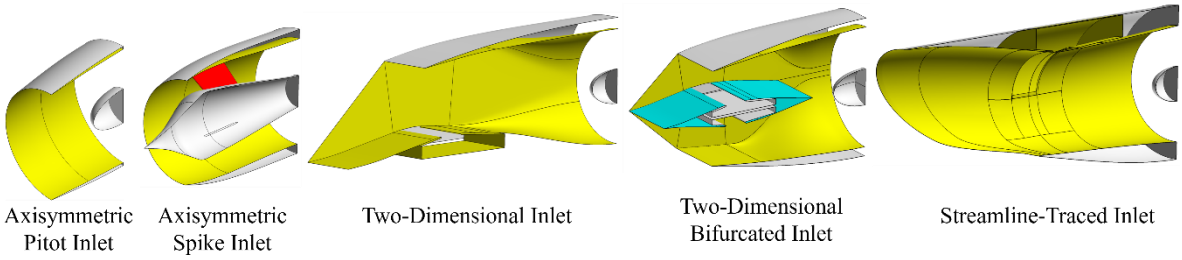

Figure 1. Types of supersonic external-compression inlets designed for Mach 1.7.

The general features of the inlets are represented in Fig. 2, which shows an image of a two-dimensional inlet for Mach 1.7. The main components of the inlets are the external supersonic diffuser, throat section, and subsonic diffuser. These components will be discussed in further detail in later sub-sections. The cowl lip starts the internal ducting of the inlet, which consists of the throat section and subsonic diffuser. The downstream end of the inlet is the engine face at which the inlet connects to the turbofan engine. The engine face includes a spinner to create an annular engine face. The inlet is assumed to be symmetric with respect to a vertical plane passing through the axis of the engine face. The cowl exterior wraps about the inlet. An axisymmetric pitot inlet does not contain an external supersonic diffuser. References [2-6] provide more detailed descriptions of the various inlets.

For the inlets of this study, the *x*-axis is horizontal in the design space with its origin coincident with the cowl lip point. The inlet axis is coincident with the *x*-axis. For the axisymmetric inlets, the *x*-axis is along the axis-of-symmetry. For the two-dimensional inlet, *x*-axis is passes through the leading edge of the external supersonic diffuser. For the streamline-traced inlet, the *x*-axis coincides with the axis-of-symmetry of the parent flowfield through which the streamline tracing is performed. The *y*-axis is vertical with a positive orientation upward and passes through the cowl lip point. The *z*-axis completes the right-hand rule with its origin on the plane-of-symmetry.

The numeric stations 0, 1, and 2 correspond to the freestream, cowl lip or entrance, and engine face stations, respectively, and are consistent with the SAE propulsion system stations [8]. Station SD is an additional station that

denotes the start of the subsonic diffuser. The following sub-sections provide details on each of the components of the inlet and the design factors that affect the design of those components.

The two-dimensional inlet depicted in Fig. 1 includes a bleed slot located at the shoulder of the bodyside or lower surface of the throat section. The shoulder point is defined where the lower surface would have a zero slope as the inlet surfaces directs the flow from the outward direction of the external supersonic diffuser back to the axial direction toward the engine face.

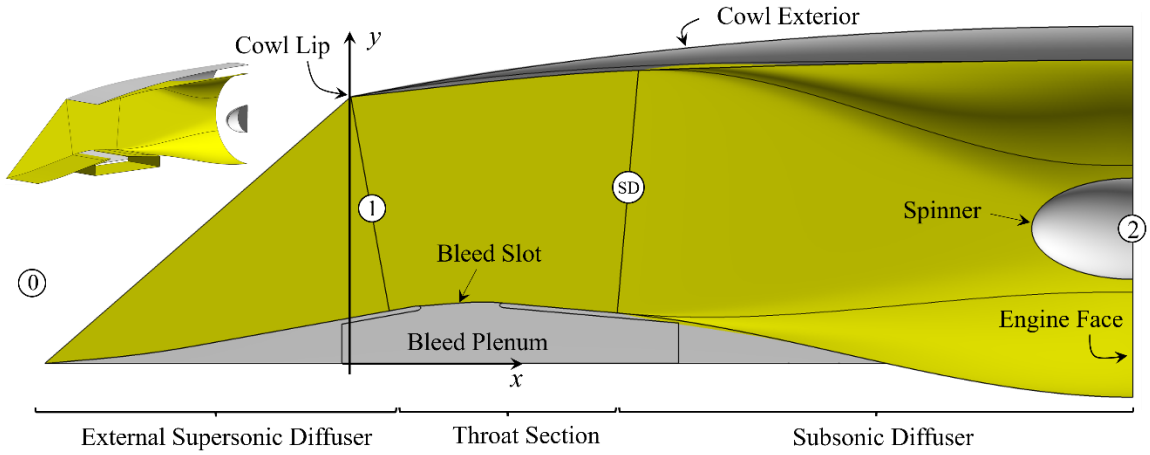

Figure 2. Description and stations of a two-dimensional inlet.

B. Freestream

Since the inlets are considered isolated without interactions with the airframe, the flow conditions at station 0 are those of the freestream. The freestream conditions form the upstream boundary conditions to the inlet design problem and include the Mach number (M_0), altitude (h_0), and angle-of-attack (α_0). For a specified altitude, the Standard Atmosphere is used to find the static pressure and temperature that define the thermodynamic state of the freestream. The angle-of-attack specifies the incidence of the inlet axis with the freestream. For this study, a zero angle-of-attack (α_0 = 0 deg) was assumed. Table 1 lists the altitudes assumed for each freestream Mach number.

Table 1. Turbofan engine-face corrected flow rates and Mach numbers.

M_0	h_0 (ft)	W_{C2} (lbm/s)	M_2
1.4	50000	413	0.663
1.7	55000	383	0.581
2.0	60000	353	0.514

C. Engine Face

The engine face forms the downstream boundary condition to the inlet design problem with the specification of the engine face geometry and the engine flow rate. The turbofan engine used for the inlet design studies is described in Ref. [1] which presents the Supersonic Technology Concept Aeroplanes (STCA). The STCA turbofan engine is based on publicly available data related to the CFM International CFM56-7B engine. The engine has a single-stage fan with a smaller diameter than that of the CFM56, but with a larger pressure ratio. The low-pressure compressor was removed to compensate for the higher ram pressure and temperatures of supersonic flight.

For the inlets of this study, the engine face was modeled as an annular cross-section with a spinner at the center. The engine-face was oriented to be perpendicular to the x-axis. The engine face had a diameter of D_2 = 3.625 feet with a spinner with a hub-to-tip ratio of D_{hub}/D_2 = 0.3. The profile of the spinner was elliptical with an aspect ratio (i.e., length-to-diameter) of 2.0. The cross-sectional area of the engine face (A_2) was formed by the circular engine face and spinner hub diameter and has cross-sectional area of A_2 = 9.3918 ft^2. Figures 1 and 2 show the shape of the engine face and spinner. The center of the engine face was positioned on the vertical plane of inlet symmetry (i.e., z_2 = 0 ft). The axial placement of the engine face (x_2) depended on the overall length of the inlet. The vertical placement of the engine face (y_2) depended on the inlet. For the axisymmetric inlets, the engine axis was coincident with the inlet axis-of-symmetry. For the two-dimensional, bifurcated inlet, the engine axis was coincident with the inlet axis located on the mirror plan of the two halves of the inlet. For the two-dimensional and streamline-traced inlets, the

engine axis could be offset in the vertical direction from the inlet axis. The offset depended on the installation of the engine. Since the inlets were isolated, the offset was chosen either to reduce the local slope variations of the internal surface of the subsonic diffuser or reduce the forward-facing surface area of the cowl exterior, which can reduce cowl wave drag. Further details on the engine face offset will be discussed in later subsections.

The engine flow rate was specified by the engine-face corrected flow rate (W_{C2}), which was set by the desired level of thrust as part of the mission of the aircraft. The values of the engine-face corrected flow rate used for the inlet designs for each freestream Mach number (M_0) are listed in Table 1. The engine-face corrected flow rate decreased with increased freestream Mach number in response to limits on the engine maximum temperature. Ref. [1] only provides data for the engine of the STCA aircraft up to $M_0 = 1.4$. The values of W_{C2} listed in Table 1 for $M_0 = 1.7$ and 2.0 were obtained using a linear extrapolation of the STCA engine data for $M_0 = 1.3$ and 1.4. The engine-face corrected flow rate corresponded to an engine-face mass-averaged Mach number (M_2), which are also listed in Table 1.

D. External Supersonic Diffuser

The external supersonic diffuser forms a compressive, supersonic flowfield in which the supersonic freestream Mach number (M_0) is decelerated to a lower supersonic Mach number (M_{EX}) at the end of the external supersonic diffuser at the cowl lip station 1. The axisymmetric pitot inlet does not have an external supersonic diffuser. The external supersonic diffusers of the axisymmetric-spike and two-dimensional inlets consist of one to three stages which create oblique shock waves and optionally, Mach waves. The surface of the external supersonic diffuser for the axisymmetric-spike inlet is formed by establishing a planar profile that is extruded about the axis-of-symmetry. Similarly, the external supersonic diffuser for the two-dimensional inlets is formed by extruding the profile in the *z*-direction. The two-dimensional inlet has a planar sidewall created with a leading edge defined by a line from the nose to the cowl lip. An illustration of the external supersonic diffuser for a two-dimensional inlet is shown in Fig. 3. The external supersonic diffuser for the streamline-traced inlet is formed from tracing streamlines through a parent flowfield, as described in references [4] and [5].

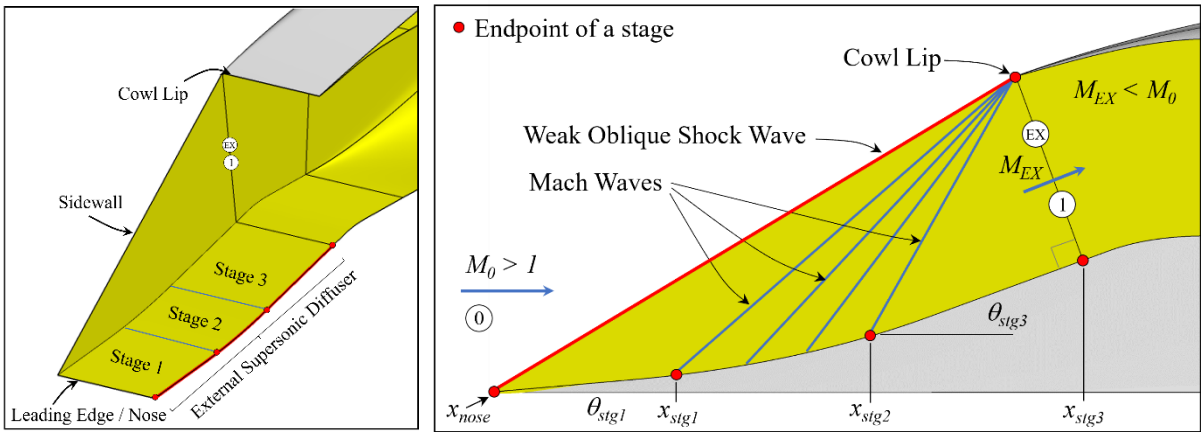

Figure 3. Model of the external supersonic diffuser of a two-dimensional inlet.

For the axisymmetric-spike and two-dimensional inlets, an important design factor for the external supersonic diffuser is the number of stages (N_{stgs}). In this work, the values explored were $N_{stgs} = 1$ or 3. The first stage is always a cone or ramp with a deflection with respect to the x-axis of θ_{stg1}, which forms an oblique shock at the nose of the inlet. For $N_{stgs} = 3$, the second stage was designed to create a system of Mach waves for isentropic compression. A second design factor is the Mach number at the end of the external supersonic diffuser (M_{EX}), which for compression $M_{EX} < M_0$ and typical values for external-compression inlets range from $1.25 \le M_{EX} \le 1.40$. The Oswatitsch condition as described in Ref. [6] is used to compute the ramp angles such that the decrease in the total pressure is the same across all the shocks. The ends of the stages are denoted by the coordinates x_{stg1}, x_{stg2}, and x_{stg3}. For the case of $N_{stgs} = 3$, the second stage used a curved surface that created a series of compressive Mach waves that are focused on the cowl lip and form an isentropic compression.

The shock and Mach waves have focal points associated with them that are placed at the *x*-coordinate of the cowl lip. At the current time, the Mach waves use the cowl lip point as their focal point. For the oblique shock waves, focal points can be specified for each shock. The placement of the focal points involves a vertical displacement (Δy_{focal}) from the cowl lip point. This displacement is calculated using a specification of the amount of supersonic

spillage ($W_{spillage}/W_{cap}$) for the inlet. The inlets of this paper use a supersonic spillage of $W_{spillage}/W_{cap}$ = 0%, which places the focal point at the cowl lip to create the "shock-on-lip" condition.

The cross-section of the external supersonic diffuser for the two-dimensional inlets is a rectangle. A reference area for the inlet is the capture area defined as $A_{cap} = y_{clip}\, w_{cap}$. Where y_{clip} is the vertical distance from the nose to the cowl lip point and w_{cap} is the width of the external supersonic diffuser. The capture flow rate (W_{cap}) is computed with the freestream conditions and the area A_{cap} and serves as the reference flow rate. The two-dimensional inlets of this paper specify that the width of the rectangular capture cross-section is equal to the engine-face diameter, $w_{cap} = D_2$.

E. Throat Section

The throat section starts at station 1 and extends to the start of the subsonic diffuser at station SD. The role of the throat section is to turn the outward flow from the external supersonic diffuser back toward the engine face and assure the formation of subsonic flow into the subsonic diffuser. The throat section of a two-dimensional inlet has cross-sections that are rectangular, and so, the centerbody and cowl interior through the throat section can be defined by planar profiles. An illustration of the geometry model for the throat section is provided in Fig. 4.

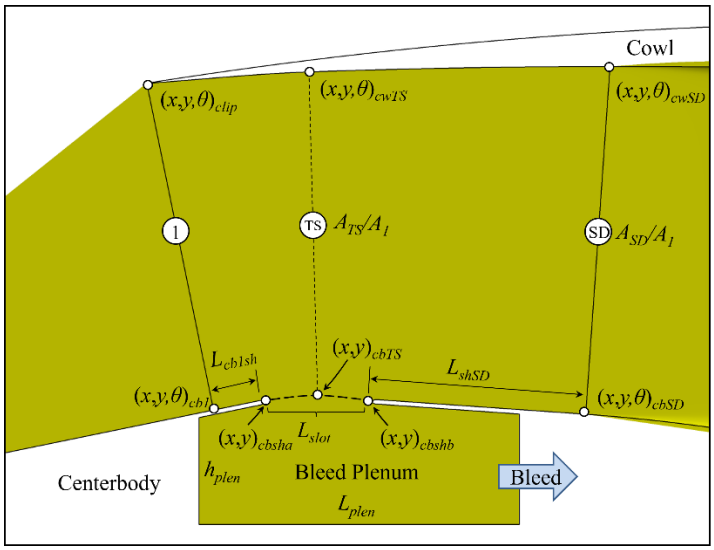

Figure 4. Model of the subsonic throat section of a two-dimensional inlet.

Point $(x,y)_{cb1}$ is the start of the throat section on the centerbody and is located on the line that intersects the cowl lip and is perpendicular to the end of the external supersonic diffuser. The slope of the centerbody at station 1 (θ_{cb1}) is set to the slope of the last stage of the external supersonic diffuser. The profile of the centerbody through the throat section consists of three planar segments. The first segment is a line of length L_{cb1sh} that starts at point $(x,y)_{cb1}$ and has a slope of θ_{cb1}. The second segment consists of a non-uniform rational B-spline (NURBS) curve that forms the shoulder or bleed slot opening. This segment changes from its initial slope of θ_{cb1} to final slope of θ_{cbSD}. The third segment is linear with a length of L_{shSD} and slope of θ_{cbSD}.

The cowl interior starts at the cowl lip point, $(x,y)_{clip}$. The profile of the cowl lip is an ellipse with the cowl lip point $(x,y)_{clip}$ being the forward-most point. The major axis of the ellipse is oriented at an angle of θ_{clip}. For a supersonic inlet, the ellipse is very small to approximate a nearly sharp cowl lip leading edge. The elliptical profile ends at the cowl lip interior point $(x,y)_{clin}$.

The profile for the cowl interior through the throat section consists of two segments. The first segment is linear with its start point at the cowl lip interior point $(x,y)_{clin}$ with a slope of $\theta_{clin} = \theta_{clip}$ and has a length of L_{cwcl}. The second segment is a planar NURBS curve that gradually changes the slope of the cowl interior profile from its initial slope of θ_{clin} to connect to the cowl interior point at station SD, $(x,y)_{SD}$ with a slope of θ_{cwSD}. The reference point $(x,y)_{cwTS}$ is located as the intersection point of the cowl interior profile and a vertical line that passes through point $(x,y)_{cbTS}$, defined as the point on the shoulder segment with a zero slope, or $\theta_{cbTS} = 0.0$. At the point $(x,y)_{cwTS}$, the cowl interior has a slope of θ_{cwTS}. The location of point $(x,y)_{cwSD}$ is fully established with the specification of the cross-sectional area at station SD (A_{SD}) that is calculated using the area ratio A_{SD}/A_1. Alternatively, the Mach number at station SD (M_{SD}) can be specified and the area ratio computed based on area-Mach number relations accounting for the bleed flow extracted within the throat section.

The throat section can accommodate a bleed slot. The slot opening occurs over the length of the shoulder and replaces the shoulder surface. A bleed slot plenum is constructed below the slot with a height (h_{plen}) and length (L_{plen}) to form a plenum that allows the slot bleed flow to reach essentially stagnant conditions.

At the design conditions for an external-compression supersonic inlet, the terminal shock is in the region of station 1. On the upstream side of the terminal shock, the Mach number is M_{EX} and for the two-dimensional external supersonic diffuser, the flow is uniform along the upstream side of the terminal shock. Downstream of the terminal shock, the Mach number (M_1) is subsonic. The terminal shock may be a normal shock or a strong oblique shock. If the cowl lip interior angle is less than the flow angle, $\theta_{clip} < \theta_{cb1}$, and the static pressure downstream of the shock is not beyond a critical value, then a strong oblique shock can be established. With a strong oblique shock, some supersonic flow likely exists within the throat section and the throat section operates to further decelerate the flow to subsonic conditions prior to arrival of the flow at station SD. The strong oblique shock approach was used for the Concorde inlet as described in Ref. [8].

F. Subsonic Diffuser

The subsonic diffuser starts at station SD and ends at the engine-face station 2. The axial length of the subsonic diffuser is L_{subd} is the primary design factor and is typically normalized by the engine-face diameter, or L_{subd}/D_2. As a general statement, a longer inlet helps the flow smoothly diffuse; however, a shorter inlet is typically desired to reduce the weight of the inlet. There also could be constraints placed on the design as to the length of the inlet.

Over the length, the subsonic diffuser transitions from the shape of the throat cross-section at station SD to a circular cross-section at station 2, which can be seen in the images of Fig. 1. For the two-dimensional inlets, the transition is from a rectangular cross-section at station SD to a circular cross-section at station 2, as illustrated in Fig. 5. The two-dimensional and streamline-traced inlets allow a vertical offset of the engine face to match the inlet up with the engine placement within the airframe. Within this study, the engine was placed mostly in line with the inlet axis to reduce curvature within the subsonic diffuser or decrease the slopes of the cowl exterior to reduce cowl wave drag. An equivalent conical angle (θ_{eqSD}) can be computed for the subsonic diffuser using the length and areas at station SD and 2.

The shaping of the surfaces of the subsonic diffuser also provides some design factors. Typically, the change in slope of the surfaces is limited to avoid localized pressure gradients that could cause boundary layer separation. The distribution of area along the length of the subsonic diffuser can be tailored. One attractive approach is to set the area distribution to achieve a linear Mach number distribution. This results in a slower rate of diffusion at the start of the subsonic diffuser where the subsonic Mach numbers are higher than at the end of the subsonic diffuser.

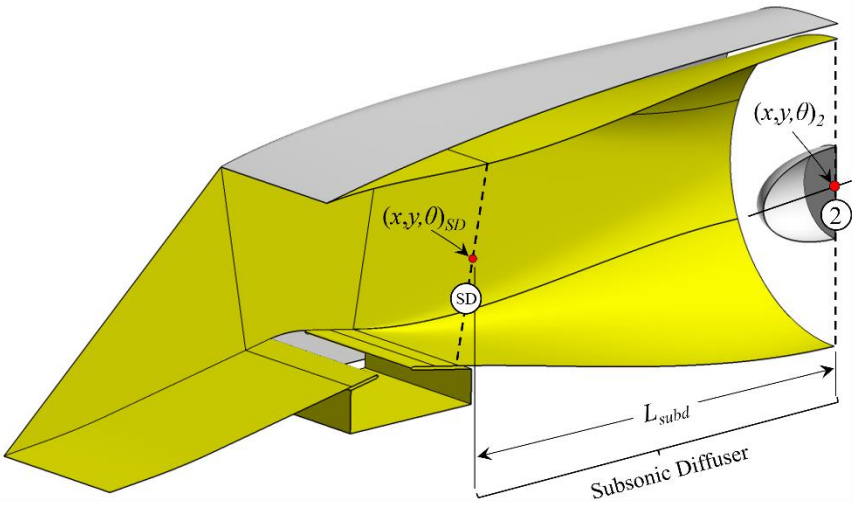

Figure 5. Model of the subsonic diffuser of a two-dimensional inlet.

G. Supersonic Inlet Design and Analysis Tool (SUPIN)

The design of the inlets was facilitated by using the Supersonic Inlet Design and Analysis Tool (SUPIN) [7]. SUPIN is a FORTRAN 95 program that reads in a text-based input data file that provides the values of the design factors. SUPIN uses analytic, empirical, and computational methods to design the inlet and estimate the flow rates,

total pressure recovery, and drag for the inlet. SUPIN generates the surfaces of the inlet and creates a Plot3D file [9] of the surface grid of the inlet. SUPIN can also automatically generate a multi-block, structured grid for a flow domain about the inlet for flow analysis using methods of computational fluid dynamics (CFD). SUPIN is available to US persons through the NASA Software Catalog (software.nasa.gov).

III. CFD Simulation Methods

The CFD simulations were performed using the Wind-US flow solver, which is discussed in the next sub-section. Subsequent sub-sections discuss the modeling of the flow domain and boundary conditions for the two-dimensional, external-compression inlets, generation of the grid, flowfield initialization, and monitoring of the flow solution for iterative convergence.

A. Wind-US Flow Solver

Wind-US [10] was used to solve the steady-state, Reynolds-averaged Navier-Stokes (RANS) equations for the flow properties at the grid points of a multi-block, structured grid defining a flow domain about the inlets. Wind-US used a cell-vertex, finite-volume representation for which the flow solution was located at the grid points and a finite-volume cell was formulated about the grid point. In Wind-US, the RANS equations were solved for the steady-state using an implicit time-marching algorithm with a first-order, implicit Euler method using local time-stepping from an initial flow solution. All the simulations were performed assuming calorically perfect air. The inviscid fluxes of the RANS equations were modeled using a second-order, upwind Roe flux-difference splitting method. The flow simulation can model inviscid flow, as well as viscous laminar or turbulent flow. For turbulent flow, the turbulent eddy viscosity was calculated using the two-equation Menter Shear-Stress Transport (SST) [11] turbulence model.

B. Computational Flow Domain and Boundary Conditions

The computational flow domain and boundary conditions (BC) used for the CFD simulations are represented by the image of Fig. 6 for the two-dimensional inlets without a bleed slot. The flow domain defined the control volume in which the RANS equations were solved. The flow domain only contained the starboard half of the inlet since the inlet had geometric symmetry about the vertical plane through the center of the inlet and flow symmetry was assumed. Symmetry boundary conditions were imposed at the geometric symmetry boundary. The internal and external surfaces of the inlet formed a portion of the boundary of the flow domain where non-slip, adiabatic viscous wall boundary conditions were imposed. The inflow and farfield boundaries of the flow domain had freestream boundary conditions imposed in which the Mach number, pressure, temperature, and angle-of-attack were specified. The inflow and farfield boundaries were positioned just upstream of the leading-edge oblique shock so that the uniform freestream conditions could be imposed on those boundaries. At the downstream end of the cowl exterior, the domain had an external outflow boundary where an extrapolation boundary condition was applied for supersonic outflow. The flow domains for the simulations of the other types of inlets are similar with slight changes and are not shown here. The flow domain for the axisymmetric spike inlet contains a singular axis upstream of the nose point.

Downstream of the engine face, a converging-diverging, outflow nozzle section was added to the flow domain to set the flow rate through the engine face. The nozzle section moved the internal outflow boundary condition downstream of the engine face, which reduced possible interference from the boundary condition on the flow at the engine face. The outflow nozzle is shown in Fig. 6. The converging-diverging segment is preceded by a constant-area segment. The length of the outflow nozzle section was twice the diameter of the engine face, which was found sufficient for the inlets of this study. The cross-sectional area of the throat was set by specifying the ratio of the diameter of the nozzle throat to the diameter of the engine-face (D_{noz}/D_2) and was set to form choked flow at the throat. Upstream of the nozzle throat and into the subsonic diffuser, the flow was subsonic and created the necessary backpressure to support the terminal shock at the throat section. Reducing the outflow nozzle throat area increased the backpressure, and so, reduced the inlet flow rate. Downstream of the outflow nozzle throat, the flow was supersonic, and so, an extrapolation boundary condition could be applied at the internal outflow boundary. The outflow nozzle section was found to create a nearly constant corrected flow rate at the engine face. This made matching the design engine-face corrected flow rate for the inlets much simpler.

When the inlet included a bleed slot, the flow domain was extended to include the slot bleed plenum. At the downstream wall of the plenum, an outflow boundary condition was specified to extract the bleed flow from the plenum. For this, a static pressure boundary condition was imposed.

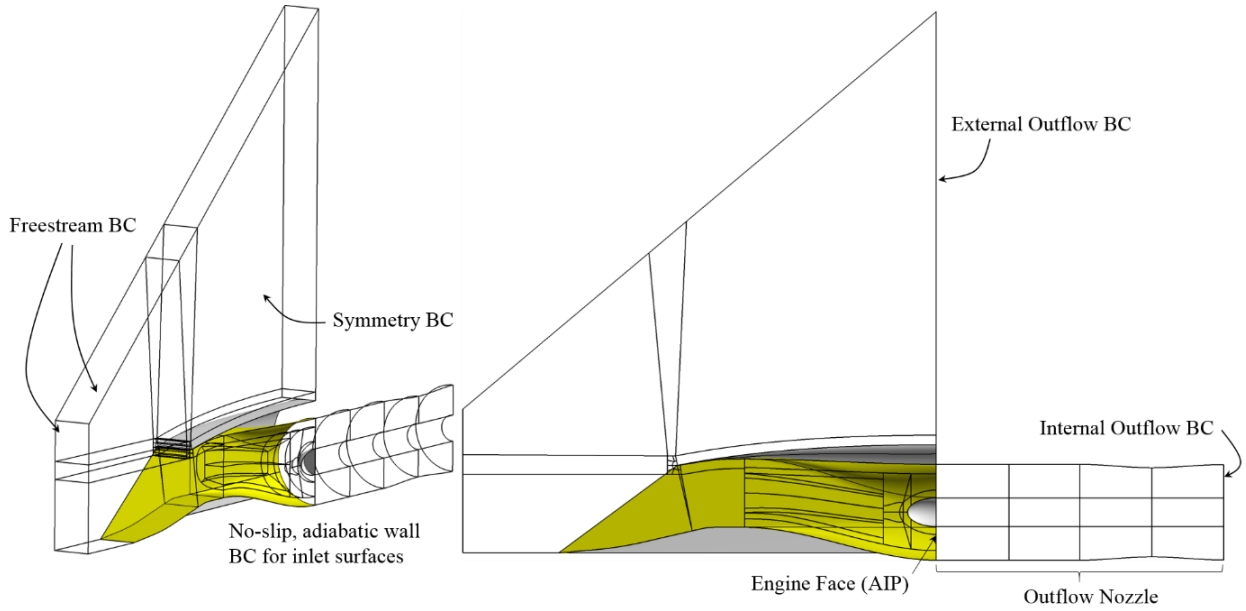

Figure 6. Flow domain and boundary conditions for a two-dimensional inlet CFD simulations.

C. Computational Grid

The computational grid for the flow domain was generated by dividing the flow domain into multiple blocks and generating structured grids for each block. SUPIN was used to generate the blocks and grid points using an automated process. SUPIN also created the boundary condition file for Wind-US. The inputs to the process include some factors to determine the extents of the flow domain and the resolution of the grid points. The grid resolution factors include the grid resolution of the first grid point away from the wall (Δs_{wall}), the grid resolution within the throat section in the streamwise direction (Δs_{thrt}), and the grid resolution at the symmetry boundary (Δs_{sym}). SUPIN then imposed these grid resolution values along the edges of the inlet geometry and flow domain to compute the required number of grid points along those edges. A grid block topology was assumed for the inlet to form the edges into faces and those faces into blocks. SUPIN generated grids along the edges, on the surfaces, and within the interior volume of each block. The interior block boundaries abutted with other block boundaries. For most blocks, the grid lines matched across block boundaries, but some non-matched boundaries were used to facilitate the structured topology. Figure 6 shows an example of the flow domain with the multi-block topology. Figure 7 shows an example of the grid lines for the block faces on the symmetry boundary. The red, blue, and green colors indicate individual faces of blocks.

D. Initial Flow Solution and Solution Monitoring

The CFD simulations were mostly initialized with a flowfield set to the freestream conditions. However, low-subsonic initial flow conditions were imposed within the bleed slot plenum. The simulation started with the first-order form of the Roe flux-splitting method to damp out large initial gradients. Eventually, the second-order flux method was applied as the residuals over the iterations decreased and the boundary layers, shock waves, and subsonic inlet flow took form. At the start of the simulations, the Courant-Friedrichs-Lewy (CFL) number had a value of 0.5 but increased incrementally to a value of 2.5 as the flow solution developed. Local time stepping was used in which the local time step used was computed based on the CFL number and the local grid cell size. The iterative convergence was indicated in part by the reduction of the root-mean-square of the residuals of the conservative variables for each block. Iterative convergence was also evaluated through the monitoring of the convergence of the inlet flow rate, total pressure recovery, and total pressure distortion. The steady-state solution was considered converged when these values changed by less than 0.001 over 1000-2000 iterations.

E. Inlet Performance Metrics

The flow solutions from the CFD simulations were used to obtain the aerodynamic performance metrics of the inlet. The four inlet performance metrics used to characterize the inlet included the inlet flow ratio (W_2/W_{cap}), the inlet total pressure recovery (p_{t2}/p_{t0}), the inlet circumferential distortion index (DPC/P), and inlet radial distortion index (DPR/P). The inlet flow ratio was defined as the inlet flow rate (W_2) divided by the reference capture flow rate (W_{cap}). The inlet flow rate (W_2) was obtained from the CFD simulation by integrating the rate of flow passing through the

cross-stream grid planes of the outflow nozzle. The total pressure at the engine face (p_{t2}) was computed as the mass-average of the total pressures at the grid plane at the engine face.

The third and fourth metrics of inlet performance were indicators of the inlet circumferential (DPC/P) and radial (DPR/P) total pressure distortion at the engine face. The distortion indices were defined on a standard 40-probe rake array and methods as defined by the Society of Automotive Engineers (SAE) Aerospace Recommended Practices (ARP) 1420 document [12]. The virtual rake array used in this study consisted of eight radial rakes each containing five total pressure probes. In the circumferential direction the eight probes were located at a constant radius and formed a ring about the circumference of the engine face. Each ring was placed radially at the centroid of equal-area sectors. The flowfield from the CFD simulation was interpolated onto the locations of the probes to obtain the total pressure at the probe location. The DPC/P indices reported in this paper were computed as the average of the DPC/P indices computed on the two inner or outer rings depending on which set of rings had the higher values of circumferential distortion. The choice of the inner or outer rings establishes whether the distortion is hub or tip distortion, respectively.

The cowl wave drag for an inlet was computed by integrating the pressures on the cowl exterior and defining the wave drag as the axial component of the resulting pressure force vector.

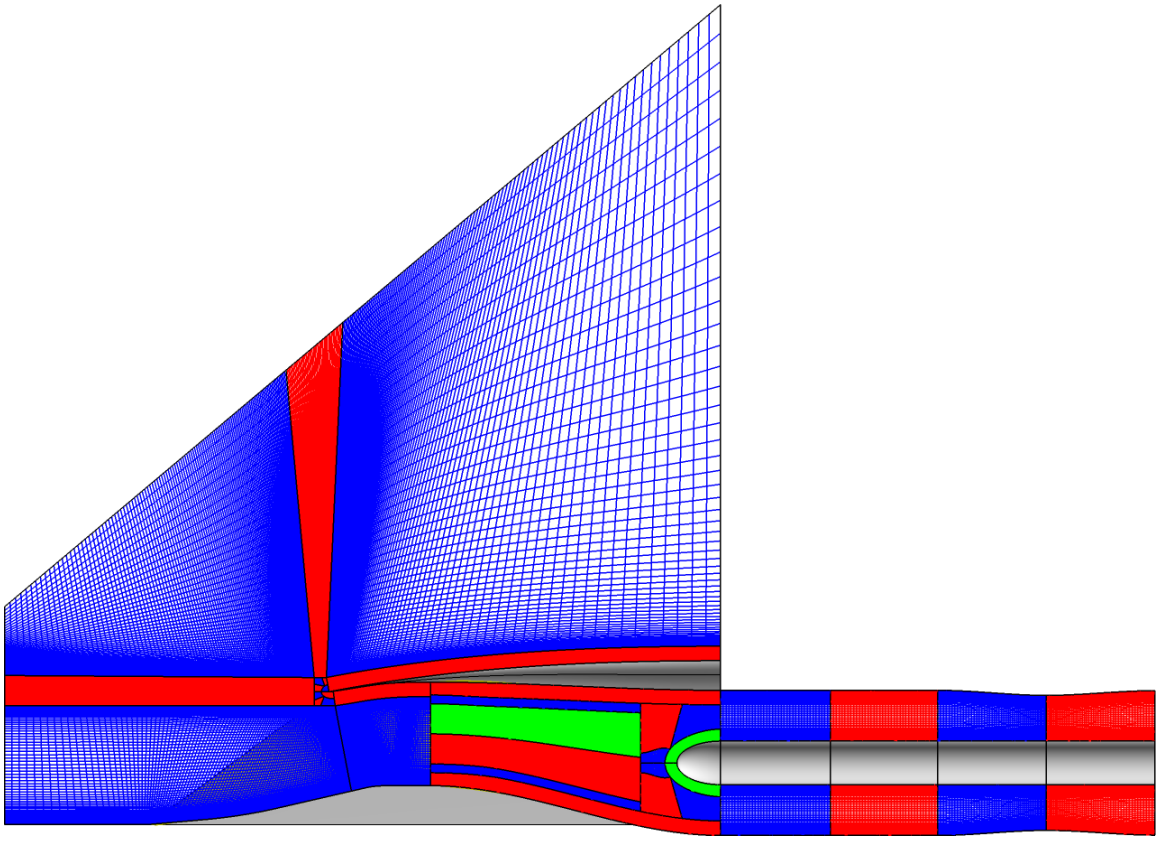

Figure 7. Structured, multi-block, computational grids on the symmetry plane for a two-dimensional inlet.

IV. Results

The design process was applied for each of the five types of inlets and at the freestream Mach numbers of M_0 = 1.4, 1.7, and 2.0 to create 15 inlets. The first subsection summarizes the design factors and geometric characteristics of the 15 inlets. Subsequent subsections provide further details for each of the inlet types. The final subsection presents a comparison of the inlet performance and some overall observations from the design study.

A. Summary of the Inlet Designs

Images of the 15 inlets are presented in Fig. 8 as side-views of the inlets cut at the vertical plane-of-symmetry at z = 0.0. Each of the 15 inlets was the result of several iterations of the inlet design for a particular freestream Mach

number and inlet type and represent the "best" inlet designed as part of this study. While a formal optimization process was not used, the design iterations involved adjustments to the design factors to maximize the inlet performance while minimizing the size of the inlets. The images of Fig. 8 were scaled so that the engine-face diameters were matched to reflect that all used the same engine-face diameter (D_2). Thus, the images provide a comparison of the overall sizes of the inlets with respect to freestream Mach number and inlet type.

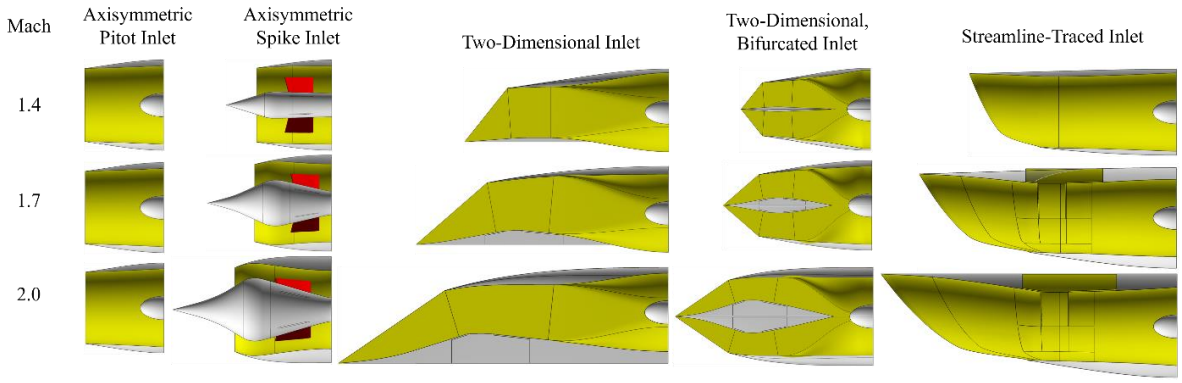

Figure 8. Images of the fifteen inlets for the freestream Mach numbers and inlet types.

Tables 2 and 3 list some of the design factors and physical dimensions of the inlets. The labels "2D Bif" and "ST" are the abbreviation for the two-dimensional, bifurcated and streamline-traced inlets, respectively. The quantities listed in boxes with a light green background indicate the design factors. Table 2 contains the design factors and properties for the external supersonic diffuser and throat section. Table 3 contains design factors and properties for the subsonic diffuser. All the lengths and areas listed in Tables 2 and 3 were normalized by the engine-face diameter (D_2) and area (A_2), respectively.

Table 2. Design factors and geometric properties of the external supersonic diffusers and throat sections. The table entries with a light green background are the specified design factors.

Type	M_0	SUPIN									
		N_{stgs}	M_{EX}	θ_{cb1}	θ_{clin}	θ_{clex}	L_{exd}/D_2	S_{comp}/A_2	M_1	L_{thrt}/D_2	θ_{cbSD}
Axi-Pitot	1.4	-	1.40	-	3.0	7.0	-	0.0	0.740	0.380	-
	1.7	-	1.70	-	1.5	8.0	-	0.0	0.641	0.001	-
	2.0	-	2.00	-	1.5	8.0	-	0.0	0.577	0.001	-
Axi-Spike	1.4	1	1.25	17.24	3.645	8.65	0.487	0.339	0.813	0.404	-1.511
	1.7	3	1.30	24.51	10.41	15.41	0.710	0.771	0.786	0.429	-12.15
	2.0	3	1.30	31.37	19.56	24.56	0.896	1.300	0.786	0.426	-15.12
2D	1.4	1	1.25	4.18	2.0	5.0	0.591	1.364	0.813	0.523	0.0
	1.7	3	1.35	11.60	6.0	11.0	1.024	2.413	0.762	0.766	-5.0
	2.0	3	1.40	17.34	12.0	17.0	1.544	3.750	0.740	1.270	-6.0
2D-Bif	1.4	1	1.25	4.14	2.0	7.0	0.296	1.098	0.813	0.370	-3.0
	1.7	3	1.35	10.21	6.0	11.0	0.512	1.932	0.762	0.423	-5.0
	2.0	3	1.40	17.34	12.0	17.0	0.772	2.982	0.740	0.568	-10.0
ST	1.4	1	1.18	-2.88	0.0	2.78	0.902	3.376	0.900	0.314	-
	1.7	1	1.27	-5.71	0.0	3.79	1.424	5.508	0.900	0.483	-
	2.0	1	1.37	-8.41	0.0	2.84	1.875	6.905	0.900	0.431	-

The specification of the design factor for the Mach at the end of the external supersonic diffuser (M_{EX}) established the slope at the end of the external supersonic diffuser (θ_{cb1}). The shock and Mach wave system and the "shock-on-lip" condition established the length of the external supersonic diffuser (L_{exd}). The surface area of the external supersonic diffuser (S_{comp}) provides a measure of the size of the external supersonic diffuser.

The specification of the design factor for the cowl lip interior angle (θ_{clin}) influenced the curve of the cowl interior for the throat section, which along with the centerbody profile, established the area through the throat section. The throat sections were designed, in general, with the geometric throat at station 1 with either a constant-area or increasing-area through the throat section. The cross-sectional area at station SD (A_{SD}) was established by specification of the design factor for the area ratio through the throat section (A_{SD}/A_1). The area A_{SD} also established

the Mach number at station SD (M_{SD}), which is listed in Table 3. The length of the throat section (L_{thrt}) was specified as a design factor. The throat sections for the axisymmetric spike and two-dimensional inlets involved turning of the flow. The amount of flow turning was established through specification of the design factor for the slope of the aft portion of the throat section (θ_{cbSD}).

The primary design factor for the subsonic diffuser was its length (L_{subd}). The subsonic diffuser length and area ratio ($A_2{*}/A_{SD}$) can be used to compute the equivalent conical diffuser angle (θ_{eqSD}).

Table 3. Design factors and geometric properties of the subsonic diffusers and overall length and surface areas of the inlets.

Type	M_0	SUPIN							
		M_{SD}	$A_2{*}/A_{SD}$	θ_{eqSD}	L_{subd}/D_2	L_{inlet}/D_2	S_{cwexx}/A_2	S_{inlet}/A_2	A_{cap}/A_2
Axi-Pitot	1.4	0.613	1.162	2.066	1.000	1.001	0.263	8.928	0.947
	1.7	0.642	1.168	2.142	1.000	1.001	0.388	8.922	0.942
	2.0	0.578	1.192	2.409	1.000	1.001	0.407	8.883	0.923
Axi-Spike	1.4	0.747	1.157	4.033	0.500	1.342	0.223	11.429	0.979
	1.7	0.702	1.211	5.217	0.500	1.585	0.454	13.287	1.081
	2.0	0.694	1.317	4.906	0.750	2.020	0.680	18.533	1.247
2D	1.4	0.721	1.216	1.780	1.500	2.591	0.120	18.361	0.953
	1.7	0.675	1.087	0.776	1.500	3.233	0.166	22.473	1.107
	2.0	0.574	1.111	0.980	1.500	4.223	0.641	31.327	1.299
2D-Bif	1.4	0.676	1.136	1.772	1.000	1.654	0.577	*18.361*	0.953
	1.7	0.607	1.087	1.164	1.000	1.906	0.705	*22.473*	1.107
	2.0	0.634	1.183	1.847	1.250	2.544	0.837	*37.413*	1.299
ST	1.4	0.831	1.209	1.729	1.500	2.643	0.357	20.254	0.972
	1.7	0.798	1.247	1.992	1.500	3.328	0.776	26.423	1.123
	2.0	0.754	1.311	2.420	1.500	3.775	0.597	29.548	1.331

Table 3 lists the surface area of the cowl exterior that projects into the axial direction (S_{cwexx}) and provides a sense of cowl wave drag that can be expected for the inlet. A larger axial area usually results in a larger cowl wave drag. The total surface area of the inlet (S_{inlet}) provides a sense of the overall size of the inlet, which may be correlated to the weight of the inlet. A reasonable goal of an inlet design is to reduce the size and weight of the inlet. The values for the inlet surface areas of the two-dimensional, bifurcated inlets shown in red and with italics are questionable values that will be corrected in the future.

The design of the inlets involves a sizing iteration in which the total pressure losses through the inlet are estimated and the capture area (A_{cap}) is adjusted until the inlet captures the amount of airflow desired by the engine at the design conditions. Table 3 lists the capture area for each inlet.

The data of Tables 2 and 3 can also be plotted. The variation of the capture areas normalized by the engine face area with respect to the freestream Mach number is plotted in the set of plots of the left-hand-side of Fig. 9. The lengths of the inlet are plotted on the right-hand-side of Fig. 9. The general trend is that the capture area and lengths increase with increasing Mach number with a nearly linear variation. The exception are the axisymmetric pitot inlets, which stay much the same. These variations can be seen in the images of the inlets of Fig. 8. The longest inlets are the two-dimensional and streamline-traced inlets, which are roughly the same length, but can be almost twice as long as the axisymmetric spike inlets. The two-dimensional, bifurcated inlet does provide a means of retaining the two-dimensional character of the inlet while resulting in a shorter inlet.

The plots of the left-hand-side of Fig. 10 compare the compressive surface area for the inlets. The compressive surface area for an external compression inlet is the surface area of the external supersonic diffuser. For the two-dimensional inlets, the surface area of the sidewall is included within the compressive surface area. The axisymmetric pitot inlets have zero compressive surface area since they do not have external supersonic diffusers. The expected trend of the inlets with external supersonic diffusers is that the compressive surface area increases in a mostly linear manner as the freestream Mach number increases. The plots indicate the streamline-traced inlets have the largest compressive area. A greater compressive surface area results in greater extent of surfaces creating boundary layers that are ingested into the inlet.

The plots of the right-hand-side of Fig. 10 show the variations of the total surface area of the inlets, which includes the surfaces of the external supersonic diffuser, throat section, subsonic diffuser, and cowl exterior. A greater total surface area may correlate with a greater weight for the inlet. As with the lengths of the inlets, the two-dimensional and streamline-traced inlets are the inlets with the greatest total surface area.

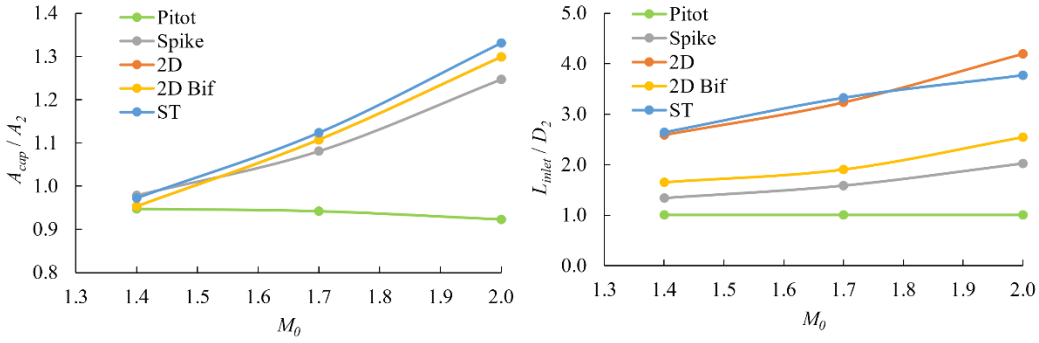

Figure 9. Variation of the capture areas and lengths of the inlets with respect to the freestream Mach number.

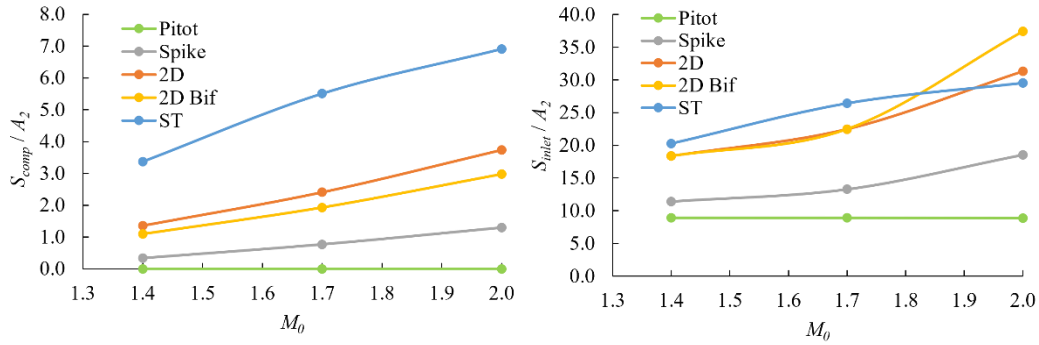

Figure 10. Variation of the compressive area and inlet surface area ratios of the inlets with respect to the freestream Mach

B. Axisymmetric Pitot Inlets

The axisymmetric pitot inlets serve as reference inlets in that they represent the simplest option for the inlet design. Numerous aircraft capable of supersonic flight have used pitot inlets with the prime example being the Lockheed Martin F-16. An image of the axisymmetric pitot inlet designed for $M_0 = 1.7$ is shown in Fig. 11. The image on the right-hand-side of Fig. 11 shows the Mach number contours from the CFD simulation for the $M_0 = 1.7$ flowfield. A normal terminal shock can be seen across the entrance of the inlet at station 1 which decelerates the flow to $M_1 = 0.641$. The normal shock is a rather stable shock in that any excess inlet flow can easily spill past the cowl lip with only a little upstream movement of the normal shock. The subsonic diffuser further diffuses the flow to $M_2 = 0.583$. Most of the losses in total pressure occur across the normal shock to yield a total pressure recovery of $p_{t2}/p_{t0} = 0.8518$. The MIL-STD-5007E document [13] provides a reasonable goal for an inlet total pressure recovery at $M_0 = 1.7$ of $(p_{t2}/p_{t0})_{MIL\text{-}STD} = 0.9489$. Thus, while a simple approach for the inlet, the pitot inlet does not provide high efficiency required of a commercial supersonic aircraft. However, the axisymmetric pitot inlet does provide a reference for the smallest inlet size and least amount of total pressure recovery.

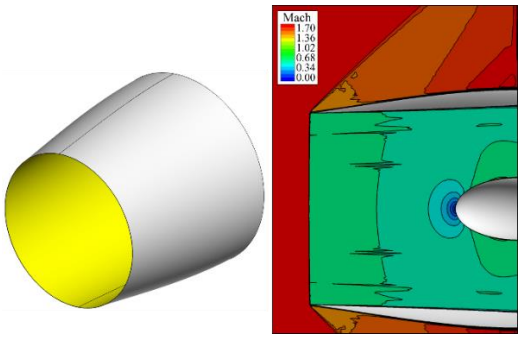

Figure 11. The axisymmetric pitot inlet for $M_0 = 1.7$ with images of the Mach number contours on the symmetry plane of the inlet.

C. Axisymmetric Spike Inlets

The axisymmetric spike inlets introduce the compressive centerbody to the axisymmetric pitot inlet to include external supersonic compression. Axisymmetric spike inlets were designed for M_0 = 1.4, 1.7, and 2.0. The axisymmetric spike inlet for M_0 = 1.7 is shown in Fig. 12.

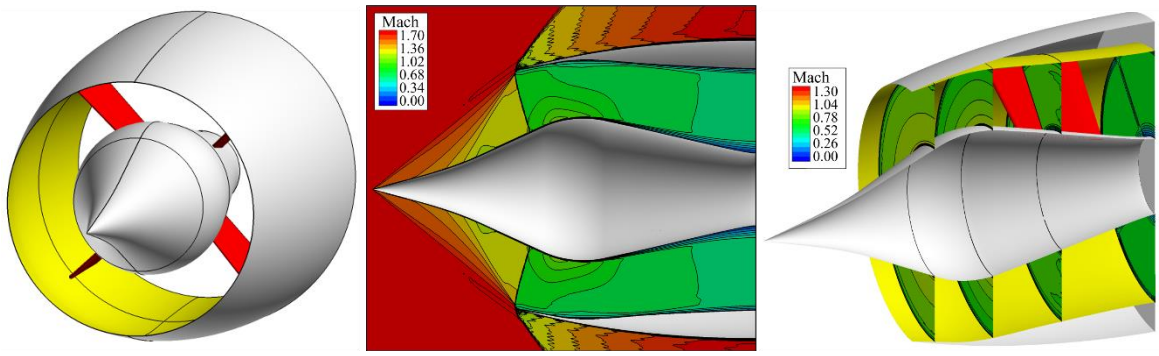

Figure 12. The axisymmetric spike inlet for M_0 = 1.7 and no bleed with images of the Mach number contours on the symmetry plane and at axial stations of the inlet.

The middle image of Fig. 12 shows the profile of the inlet along with Mach number contours from a CFD simulation at M_0 = 1.7. The external supersonic diffuser was designed with three stages in which the second stage creates Mach waves. The nose conical shock and the Mach waves all focus onto the cowl lip point. The throat section was designed to gradually turn the flow toward the engine face. One approach is to use a circular arc for the centerbody within the throat section; however, through iterations on the design, it was found that a shorter throat section worked effectively as shown by the Mach contours for Fig. 12. The design process also involved reducing the length of the subsonic diffuser to a final length of L_{subd}/D_2 = 0.5 for the Mach 1.7 inlet. The Mach number contours show the normal terminal shock placed at the inlet entrance at station 1. The image on the right-hand-side of Fig. 12 shows Mach number contours at axial stations through the throat section and subsonic diffuser. The contours show the boundary layers thickening through the inlet. The inlet contains four support struts that secure the centerbody with the cowling. The Mach contour at the engine face show the disturbance in the flow at the wake from the end of the support struts. The aerodynamic performance of the axisymmetric spike inlet is summarized below.

D. Two-Dimensional Inlets

The lessons of Reference [2] were applied to the design of the two-dimensional inlets. Tables 2 and 3 list some of the design factors used within SUPIN to create the inlets. The external supersonic diffuser for the inlet for M_0 = 1.4 had only a single-stage ramp while the inlets for M_0 = 1.7 and 2.0 had three stages with the second stage being a curved isentropic section. The inlet for M_0 = 2.0 forms a strong oblique shock much in the manner of the inlet for the Concorde aircraft [13]. The cowl lip interior angles, θ_{clin}, were set to be at or slightly below the local flow angle at the cowl lip. The throat sections were specified to turn the flow back toward the engine face but involved a gradually increasing cross-sectional area through the throat section.

The inlet for M_0 = 2.0 is shown on the left of Fig. 13. A bleed slot was used to create a strong oblique terminal shock with a design factor of M_{EX} = 1.40. The upper image on the right-hand-side of Fig. 13 shows the Mach contours on the symmetry plane and show that at the critical operating condition, a strong oblique terminal shock is formed at the entrance station 1. The inlet yielded good performance, which is summarized in the last subsection. A feature of two-dimensional inlets is the formation of a vortex in the lower corners. The vortex seems to originate by the deflection downward of the flow on the sidewall downstream of the terminal shock. This downward flow forms the vortex when the flow reaches the lower ramp surfaces. The bleed slot helps to reduce the adverse effects of this vortex. As the vortex propagates downstream, it is diffused somewhat by the subsonic diffuser.

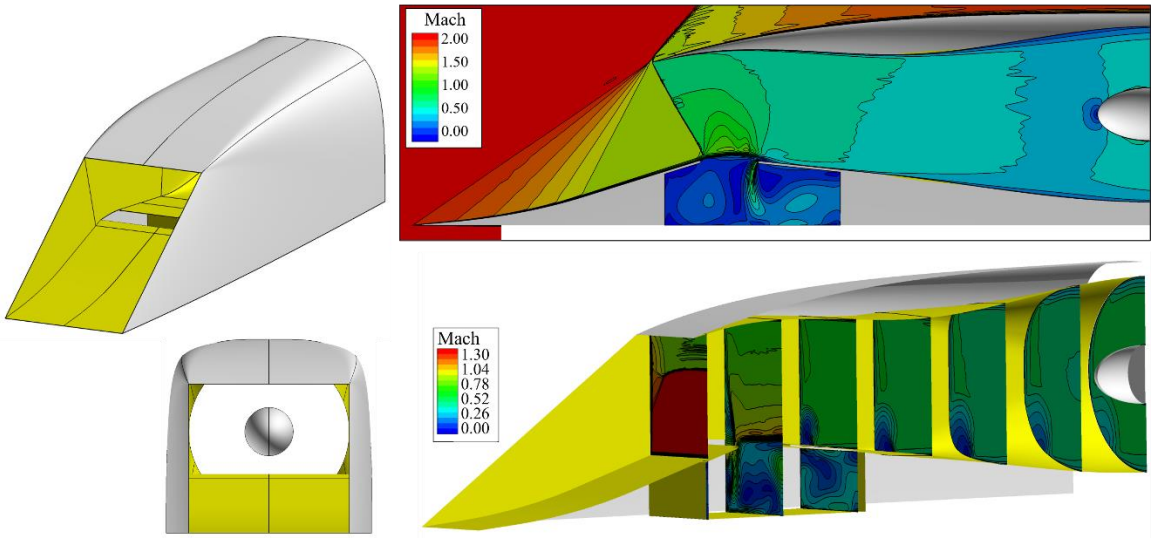

Figure 13. The two-dimensional inlet for M_0 = 2.0 and 5% slot bleed with images of the Mach number contours on the symmetry plane and at axial stations of the inlet.

E. Two-Dimensional, Bifurcated Inlets

The two-dimensional bifurcated inlets are formed by mirroring two-dimensional inlets about the horizontal plane through the inlet axis. Each half has its own external supersonic diffuser and throat section with their bleed slots and plenums. Within SUPIN, the two-dimensional, bifurcated inlets are designed using the same methods as the two-dimensional inlets, except the sizing is performed using half of the engine face as the sizing for the two-dimensional inlets. In modeling the subsonic diffuser, the centerbody ends before the start of the spinner so that both halves of the inlet have a common mixing region ahead of the engine face. Images of the two-dimensional, bifurcated inlet for M_0 = 1.7 are shown in Fig. 14. As discussed previously, the two-dimensional, bifurcated inlet provides a means of having a two-dimensional inlet while reducing the length as compared to the regular two-dimensional inlet. CFD simulations of the two-dimensional, bifurcated inlets have not yet been performed.

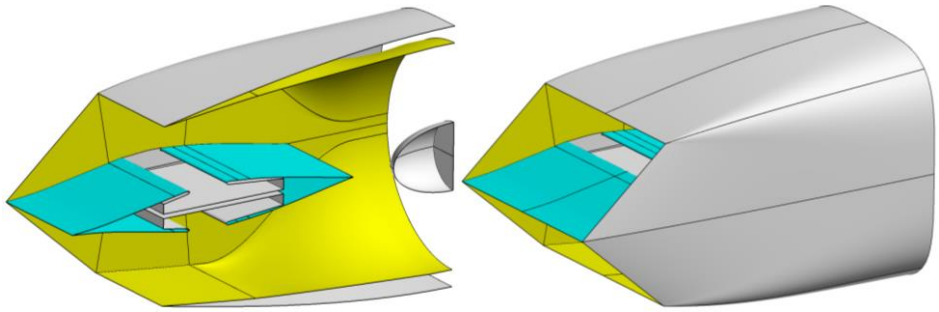

Figure 14. The two-dimensional, bifurcated inlet for M_0 = 1.7.

F. Streamline-Traced Inlets

The streamline-traced inlets use an axisymmetric, inward-turning parent flowfield to form the external supersonic diffuser through streamline tracing. STEX inlets were designed for M_0 = 1.4, 1.7, and 2.0 using a circular tracing curve to create a round inlet. The inlets feature a scarfed leading edge due to an offset of the tracing curve above the axis-of-symmetry. This provides a cut-out for spillage of subsonic flow at the downstream portion of the leading edge. The images of the inlet for M_0 = 2.0 are shown in Fig. 15. The inlet contains a bleed slot at the shoulder of the inlet.

The images on the right-hand-side in Fig. 15 show Mach number contours on the symmetry plane and at axial stations. The leading-edge shock and Mach waves are illustrated in the Mach contours. The terminal shock wraps about the cowl lip at the bottom of the inlet and projects downstream into the inlet. The angle of the terminal shock indicates that it is a strong oblique shock. The terminal shock interacts with the bleed slot and forms a small supersonic region that terminates with a small normal shock at the end of the bleed slot. This shock structure is the same as

observed with the Concorde inlet [6] and previous streamline-traced inlet studies [5]. The Mach number contours along the axial stations show a region of low-momentum flow at the top of the subsonic diffuser that propagates to the engine face. This low-momentum region was present in earlier studies [4,5] for streamline-traced inlets generated using circular tracing curves. An alternative to the circular inlet is the "flattop" inlet discussed in Ref. [5] in which inlets for M_0 = 2.0 were designed with the streamline-tracing curves that were flattened along the top tracing curve. This created a flattened top surface for the streamlined surface and throat section. The "flattop" inlets did show a slight decrease in the inlet total pressure recovery but may integrate better with wing or fuselage surfaces than the circular inlets.

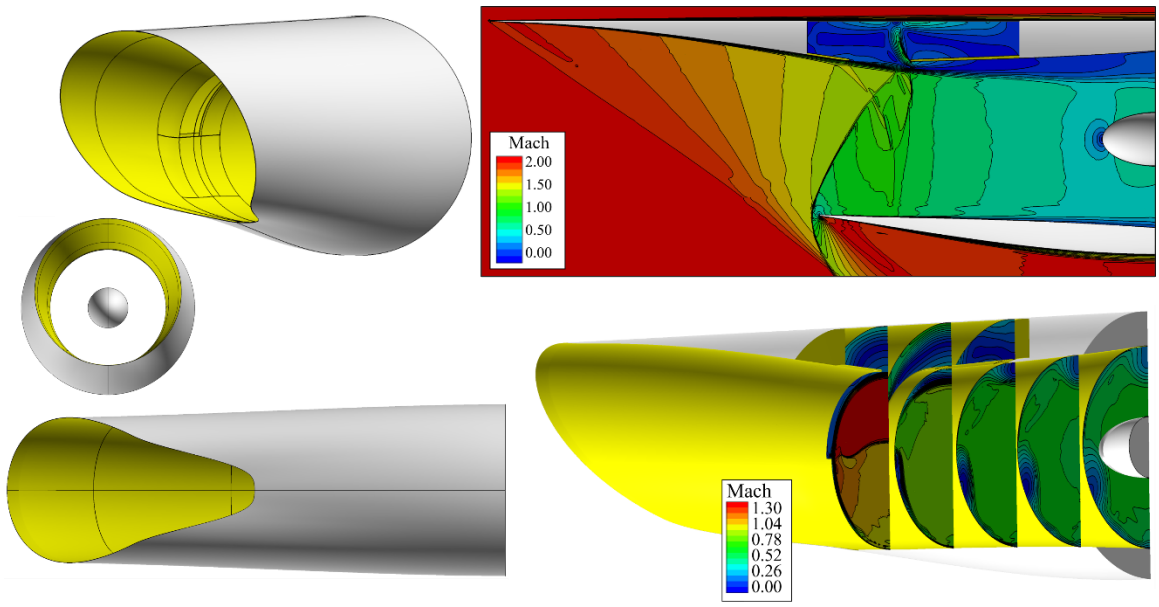

Figure 15. The streamline-traced inlet for M_0 = 2.0 and 5% slot bleed with the Mach number contours on the symmetry plane and at axial stations of the inlet.

G. Summary of the Aerodynamic Performance of the Inlets

This subsection summarizes the inlet aerodynamic performance of the 15 inlets as characterized by the inlet flow rates, wave drag, and total pressure recovery and distortion. The estimates of the performance metrics obtained from SUPIN are compared to those from CFD simulations. The performance is first examined at the critical operating condition in which the inlet flow rate and conditions provides the design corrected flow rate. The performance is then examined for the variation of the inlet engine-face flow rate at the design freestream Mach number to establish the characteristic curves for the inlet. CFD simulations have not yet been performed for the two-dimensional, bifurcated inlets, but will be performed in the future.

The inlet spillage, bleed, and engine-face flow ratios for the inlet operating at the critical operating points are listed in Table 4. All the inlets were designed for zero subsonic and supersonic spillage; however, some level of spillage was observed from the CFD simulations with the streamline-traced inlets showing the greatest level of spillage. The two-dimensional and streamline-traced inlets were designed with bleed slots and 3% and 5% bleed for M_0 = 1.7 and 2.0, respectively. The axisymmetric spike inlets were not designed with bleed, but bleed is likely needed for the M_0 = 2.0 axisymmetric spike inlet to limit the occurrence of buzz at subcritical conditions. The engine-face flow ratio completes the flow balance through the inlet.

The total pressure recoveries, static pressure ratios, and wave drag coefficients are listed in Table 5 for the inlets operating at the critical flow conditions. The indices for the radial and circumferential distortion as obtained from the CFD simulations is also listed in Table 5.

Some of the data of Tables 5 for the CFD simulations are plotted in Figs. 16, 17, and 18. The plots of the total pressure recoveries on the left-hand-side of Fig. 16 suggests that similar recovery can be obtained from either the axisymmetric spike, two-dimensional, or streamline-traced inlets. The plots of the wave drag coefficients on the right-hand-side of Fig. 16 show that the inward-turning nature of the streamline-traced inlets results in lower wave drag coefficients. The plots of the static pressure ratio on the left-hand-side of Fig. 17 show similar inlet pressurizations for the inlets. As mentioned previously, the streamline-traced inlets show the highest spillage as shown in the plots

on the right-hand-side of Fig. 17. The plots of Fig. 18 show the variation of the radial and circumferential total pressure distortion indices as computed from the CFD simulations. The upper limit of DPR/P = DPC/P = 0.10 is also plotted and all indices of the inlets are below the limit. The higher distortion indices for the Mach 1.4 two-dimensional inlet does not seem consistent with the values for the Mach 1.7 and 2.0 two-dimensional inlets, which suggests that those indices could be reduced. The higher distortion levels for the streamline-traced inlets were likely due to the low-momentum region that formed at the top of the subsonic diffuser of those inlets. None of the inlets employed vortex generators in the subsonic diffuser which could further reduce total pressure distortion.

Table 4. Flow ratios for the inlets at the critical operating points.

Type	M_0	SUPIN			CFD		
		$W_{spillage}/W_{cap}$	W_{bleed}/W_{cap}	W_2/W_{cap}	$W_{spillage}/W_{cap}$	W_{bleed}/W_{cap}	W_2/W_{cap}
Axi-Pitot	1.4	0.0	0.0	1.00	0.0023	0.0000	0.9977
	1.7	0.0	0.0	1.00	0.0024	0.0000	0.9976
	2.0	0.0	0.0	1.00	0.0002	0.0000	0.9998
Axi-Spike	1.4	0.0	0.0	1.00	0.0083	0.0000	0.9917
	1.7	0.0	0.0	1.00	0.0184	0.0000	0.9816
	2.0	0.0	0.0	1.00	0.0155	0.0000	0.9845
2D	1.4	0.0	0.0	1.00	0.0047	0.0000	0.9953
	1.7	0.0	0.03	0.97	0.0109	0.0314	0.9577
	2.0	0.0	0.05	0.95	0.0124	0.0500	0.9376
2D Bif	1.4	0.0	0.0	1.00	-	-	-
	1.7	0.0	0.03	0.97	-	-	-
	2.0	0.0	0.05	0.95	-	-	-
ST	1.4	0.0	0.0	1.00	0.0099	0.0000	0.9901
	1.7	0.0	0.03	0.97	0.0237	0.0300	0.9463
	2.0	0.0	0.05	0.95	0.0338	0.0500	0.9162

Table 5. Inlet performance data for the inlets at the critical operating condition.

Type	M_0	SUPIN				CFD					
		M_2	p_{t2}/p_{t0}	p_2/p_0	C_{Dwave}	M_2	p_{t2}/p_{t0}	p_2/p_0	C_{Dwave}	DPC/P	DPR/P
Axi-Pitot	1.4	0.663	0.9545	2.261	0.1037	0.667	0.9529	2.247	0.1008	0.0000	-
	1.7	0.581	0.8531	3.350	0.0830	0.583	0.8518	3.337	0.0834	0.0000	-
	2.0	0.514	0.7190	4.699	0.0758	0.516	0.7181	4.680	0.0788	0.0000	-
Axi-Spike	1.4	0.663	0.9820	2.346	0.0963	0.6680	0.9776	2.3000	0.0956	0.0251	0.0016
	1.7	0.581	0.9744	3.478	0.1174	0.5888	0.9616	3.7283	0.1237	0.0179	0.0264
	2.0	0.514	0.9714	5.954	0.1707	0.5262	0.9540	6.1224	0.2001	0.0116	0.0244
2D	1.4	0.663	0.9749	2.315	0.1290	0.6840	0.9541	2.1959	0.1499	0.0744	0.0876
	1.7	0.581	0.9380	3.813	0.0772	0.5834	0.9611	3.7603	0.0795	0.0263	0.0399
	2.0	0.514	0.9467	6.349	0.1039	0.5166	0.9487	6.1705	0.1095	0.0229	0.0349
2D Bif	1.4	0.663	0.9804	2.372	0.0975	-	-	-	-	-	-
	1.7	0.581	0.9632	3.663	0.0615	-	-	-	-	-	-
	2.0	0.514	0.9500	5.988	0.0531	-	-	-	-	-	-
ST	1.4	0.663	0.9887	2.365	0.0166	0.671	0.9709	2.274	0.0145	0.0154	0.0715
	1.7	0.581	0.9813	3.746	0.0397	0.591	0.9698	3.746	0.0351	0.0656	0.0695
	2.0	0.500	0.9686	6.086	0.0169	0.526	0.9495	6.093	0.0187	0.0452	0.0599

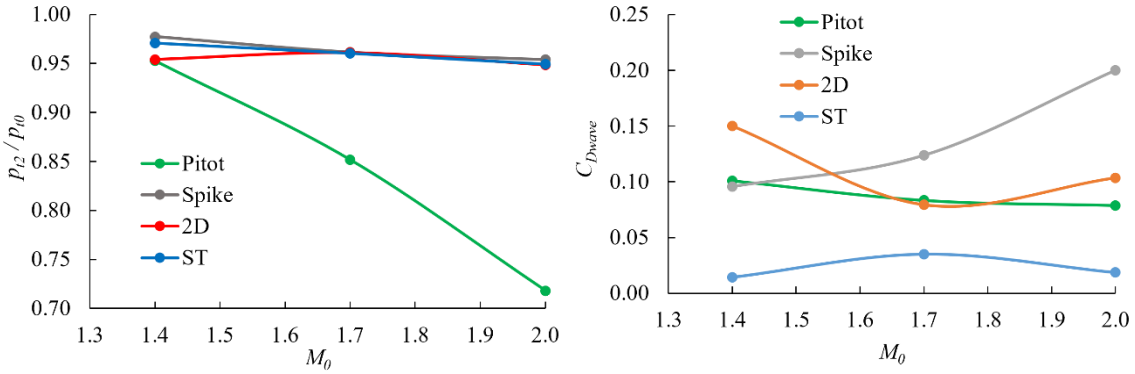

Figure 16. Variation of the total-pressure recovery (left) and wave drag (right) for the inlets at the critical operating condition with respect to the freestream Mach number.

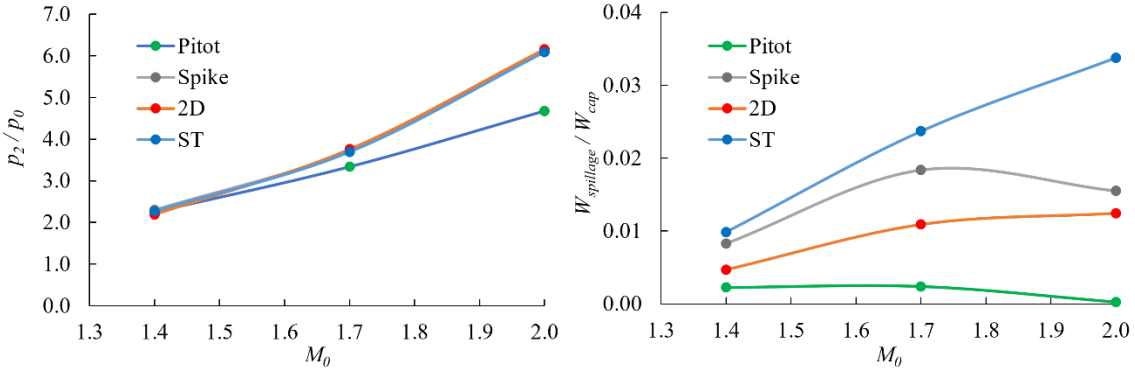

Figure 17. Variation of the static pressure ratio (left) and spillage flow ratio (right) for the inlets at the critical operating condition with respect to the freestream Mach number.

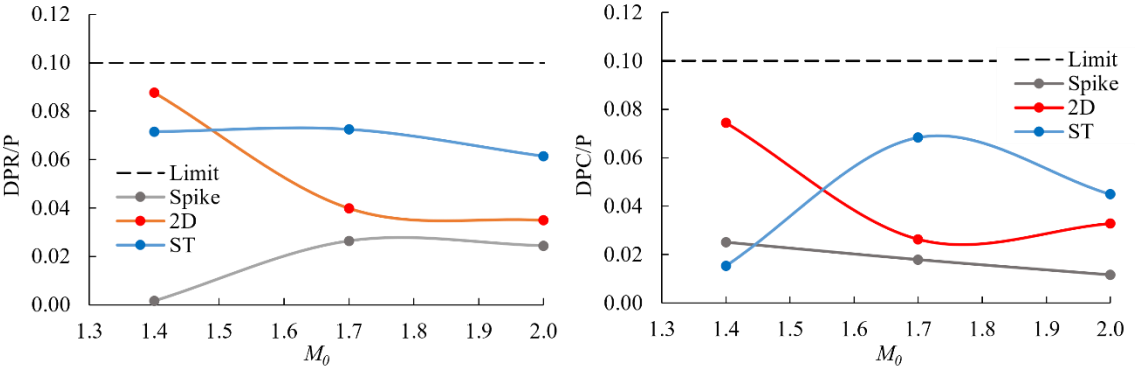

Figure 18. Variation of the radial (left) and circumferential (right) total-pressure distortion for the inlets at the critical operating condition with respect to the freestream Mach number.

The characteristic curves for the inlets show the variation of the total pressure recovery (p_{t2}/p_{t0}), radial distortion (DPR/P), and circumferential distortion (DPC/P) with respect to the engine-face flow ratio (W_2/W_{cap}). The characteristic curves are obtained from CFD simulations and Fig. 19 shows the curves. The vertical portion of the curves indicates a constant flow ratio and is the supercritical leg of the curve. As the terminal shock moves forward of the cowl lip plane and spills subsonic flow or the bleed increases, the engine-face flow ratio decreases and forms the subcritical leg of the curve. The critical operating point was designed to occur with the condition of maximum total pressure recovery with maximum engine-face flow ratio.

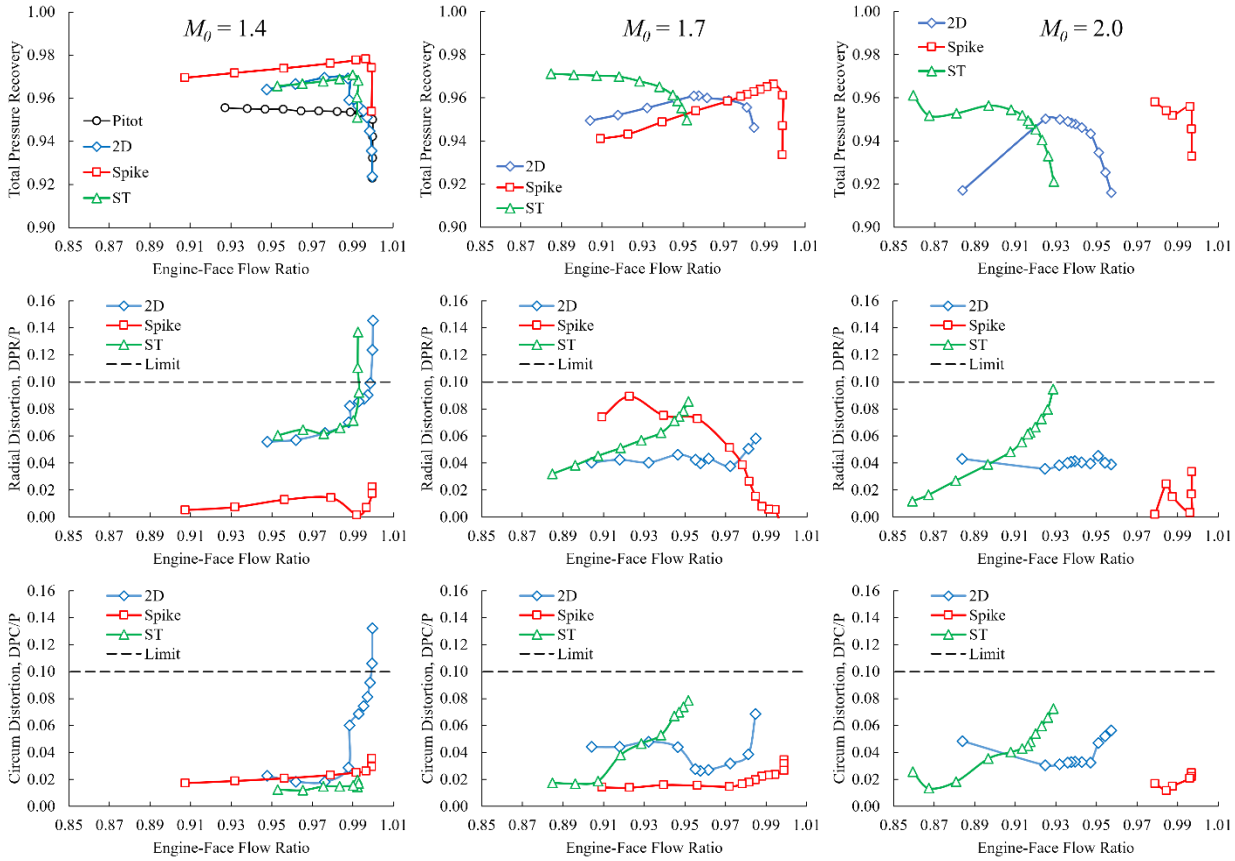

Figure 19. Characteristic curves for the total pressure recovery, radial distortion, and circumferential distortion with respect to engine-face flow ratio.

V. Conclusion

Fifteen supersonic external-compression inlets were designed for the cruise conditions for the combination of three freestream Mach numbers of M_0 = 1.4, 1.7, and 2.0 and the five inlet types, which were the axisymmetric pitot, axisymmetric spike, two-dimensional, two-dimensional bifurcated, and streamline-traced inlets. Their physical dimensions and aerodynamic performance were discussed and compared. For each inlet, the engine-face flow ratio was varied to create the characteristic curves for the total pressure recovery and the radial and circumferential total pressure distortion indices. Some conclusions from the study are:

- Similar levels of the total pressure recovery seem to be achievable for the inlets with an external supersonic diffuser regardless of the inlet type.
- The streamline-traced inlet has much lower wave drag than the other types of inlets.
- The use of a strong oblique terminal shock for the two-dimensional inlets for freestream Mach number of M_0 = 2.0 resulted in lower wave drag than for the axisymmetric spike inlet.
- The streamline-traced inlet had 1 to 3% percent greater spillage than the other inlets, which was compensated by increasing the size of the capture area.
- All inlets captured about the same amount of airflow at each freestream Mach number.
- The total pressure radial and distortion indices were within their limits at the design condition. The use of vortex generators within the subsonic diffuser could reduce distortion further below the limit.
- The axisymmetric spike inlet is an attractive inlet for Mach 1.4 to 1.7 because of its compact size and stable shock system.

- Above Mach 1.7 to Mach 2.0, the two-dimensional inlets are likely more attractive than the axisymmetric spike inlets due to lower wave drag. The use of a bifurcated, two-dimensional inlet could make the inlet more compact than the two-dimensional inlet.
- The streamline-traced inlet could be more attractive than the two-dimensional inlets closer to Mach 2 due to the lower wave drag.

Future studies will examine the aerodynamic performance of the inlets at off-design conditions that include the inlet at angle-of-attack and angle-of-sideslip, as well as at take-off, approach-to-landing, and transonic conditions. Such studies would examine variable-geometry, including auxiliary inlets, for matching engine flow demands at these conditions.

Acknowledgments

This work was funded by the NASA Commercial Supersonic Technology (CST) Project.

References

[1] Berton, J. J., Huff, D. L., Seidel, J. A., and Geiselhart, K. A., "Supersonic Technology Concept Aeroplanes for Environmental Studies," AIAA Paper 2020-0263, January 2020.

[2] Slater, J. W., "Design Factors for Two-Dimensional, External-Compression Supersonic Inlets," AIAA Paper 2020-2090, January 2020.

[3] Howerton, L. W. and Slater, J. W., "Auxiliary Inlet Design Study for Mach 1.4," AIAA Paper 2021-3548, August 2021.

[4] Slater, J. W., "Refinement of Vortex Generators in a Streamline-Traced, External-Compression Supersonic Inlet," AIAA Paper 2019-4423, August 2019.

[5] Slater, J. W., "Streamline-Traced, External-Compression Supersonic Inlets for Mach 2", ISABE Paper 2022-0278, September 2022.

[6] Slater, J. W., "A Study of the Internal Aerodynamics of the Concorde Inlet," AIAA Paper 2020-3770, August 2020.

[7] Slater, J. W., "SUPIN: A Computational Tool for Supersonic Inlet Design," AIAA Paper 2016-0532, January 2016.

[8] Society of Automotive Engineering (SAE), "Aircraft Propulsion System Performance Station Designation and Nomenclature," Aerospace Standard (AS) 755, December 1997.

[9] Walatka, P. P., Buning, P. G., Pierce, L., and Elson, P. A., "PLOT3D User's Manual," NASA-TM-101067, March 1990.

[10] Yoder, D. A., 'Wind-US User's Guide: Version 3.0," NASA TM 2016-219078, March 2016.

[11] Menter, F. R., "Two-Equation Eddy-Viscosity Turbulence Models for Engineering Applications," *AIAA Journal*, Vol. 32, No. 8, 1994, pp. 1598–1605. doi: 10.2514/3.12149.

[12] Society of Automotive Engineers (SAE), "Gas Turbine Engine Inlet Flow Distortion Guidelines," SAE ARP 1420, Rev. C, April 2017.

[13] MIL-STD-5007E, "Engines, Aircraft, Turbo-Jet, and Turbofan, Model Specifications For," September 1983.